El Niño–La Niña Asymmetry in the Coupled Model Intercomparison Project Simulations*

SOON-IL AN

International Pacific Research Center, University of Hawaii at Manoa, Honolulu, Hawaii

YOO-GEUN HAM AND JONG-SEONG KUG

School of Earth and Environmental Science, Seoul National University, Seoul, South Korea

FEI-FEI JIN

Department of Meteorology, The Florida State University, Tallahassee, Florida

IN-SIK KANG

School of Earth and Environmental Science, Seoul National University, Seoul, South Korea

(Manuscript received 7 July 2004, in final form 25 January 2005)

ABSTRACT

The El Niño–La Niña asymmetry was estimated in the 10 different models participating in the Coupled Model Intercomparison Project (CMIP). Large differences in the "asymmetricity" (a variance-weighted skewness) of SST anomalies are found between models and observations. Most of the coupled models underestimate the nonlinearity and only a few exhibit the positively skewed SST anomalies over the tropical eastern Pacific as seen in the observation. A significant association between the nonlinear dynamical heating (NDH) and asymmetricity in the model–ENSO indices is found, inferring that asymmetricity is caused mainly by NDH. Among the 10 models, one coupled GCM simulates the asymmetricity of the tropical SST realistically, and its simulation manifests a strong relationship between the intensity and the propagating feature of ENSO—the strong ENSO events moving eastward and the weak ENSO events moving westward—which is consistent with the observation. Interestingly, the coupled general circulation models, of which the ocean model is based on the one used by Bryan and Cox, commonly showed the reasonably positive skewed ENSO.

The decadal changes in the skewness, variance, and NDH of the model-simulated ENSO are also observed. These three quantities over the tropical eastern Pacific are significantly correlated to each other, indicating that the decadal change in ENSO variability is closely related to the nonlinear process of ENSO. It is also found that these decadal changes in ENSO variability are related to the decadal variation in the tropical Pacific SST, implying that the decadal change in the El Niño–La Niña asymmetry could manifest itself as a rectified change in the background state.

* School of Ocean and Earth Science and Technology Contribution Number 6547 and International Pacific Research Center Contribution Number 312.

Corresponding author address: Dr. Soon-Il An, International Pacific Research Center, SOEST, University of Hawaii at Manoa, Honolulu, HI 96822.
E-mail: sian@hawaii.edu

1. Introduction

In the 1980s, the advent of simple and intermediate coupled models brought about a view that the El Niño–Southern Oscillation (ENSO) could be cyclic (McCreary 1983; Cane and Zebiak 1985; Battisti and Hirst 1989), different from the earlier speculation that each ENSO could be an independent event (Bjerknes 1969; Wyrtki 1975, 1985). Since then, early "delayed oscillator" (Schopf and Suarez 1988; Battisti and Hirst 1989), latter "recharge oscillator" (Jin 1996, 1997), "advective-reflective oscillator" (Picaut et al. 1997), and "western Pacific oscillator" (Weisberg and Wang 1997) provided a comprehensive idea regarding this cyclic nature of ENSO [also see Wang (2001) for the summary of all ENSO conceptual models]. However, some observational studies have pointed out that while the termination of El Niños has occurred consistently with a strong canonical feature, their initiation is less obvious (Kessler and McPhaden 1995). Furthermore, Thompson and Battisti (2000, 2001) showed that the basic features of ENSO could be reproduced from the linear model subjected to the stochastic forcing, meaning that the essential characteristics of ENSO appear to be governed by a linear process and the resultant ENSO must be sporadic. In other words, the climate study community is still struggling to get a consensus as to whether ENSO is a large-scale deterministic system with nonlinearity (Jin et al. 1994; Tziperman et al. 1994) or is a linear system subjected to stochastic forcing (Penland and Sardeshmukh 1995; Chang et al. 1996; Moore and Kleeman 1999; Thompson and Battisti 2000, 2001). Nevertheless, recently Jin et al. (2003) and An and Jin (2004) have measured the observed ENSO nonlinearity not only via a statistical method (skewness) but also via a dynamical venue such as nonlinear dynamical heating (NDH), and pointed out that the ENSO has strong nonlinearity that causes the asymmetry between El Niño and La Niña. Actually, Thompson and Battisti (2001) failed to produce the asymmetry of ENSO from their model simulations because of the lack of the nonlinearity. Although it is still unclear whether ENSO is stable or unstable, the nonlinearity of ENSO yields intrinsic features that are beyond description by a linear dynamics subjected to the stochastic forcing.

Concurrent with the late 1970s climate shift, the general characteristics of ENSO changed (Wang 1995; An and Jin 2000; Fedorov and Philander 2000; An and Wang 2000; Wang and An 2001). Moreover, the positive skewness of the ENSO index, indicating El Niño being stronger than La Niña, increased since the late 1970s (An 2004). This asymmetry between El Niño and La Niña was also objectively identified by using the nonlinear principal component analysis (NLPCA), which detects a low-dimensional nonlinear structure in multivariate datasets (Hsieh 2001, 2004; Wu and Hsieh 2003). The nonlinear principal mode showed not only the asymmetry in amplitude but also the asymmetry in the corresponding spatial patterns of oceanic and atmospheric variables associated with El Niño and La Niña. Furthermore, An and Jin (2004) pointed out that the asymmetry of ENSO was due to the nonlinear dynamical thermal advections in the oceanic surface layer (i.e., NDH), which also increased after the late 1970s.

The evidence regarding the ENSO nonlinearity so far is mainly deduced from short observational records with limited statistics. Here we take an alternative approach: namely, the analysis of the coupled general circulation model (CGCM) outputs obtained from the Coupled Model Intercomparison Project (CMIP; see Table 1). The coupled ocean–atmosphere models, to some extent, can capture some aspects of the observed ENSO. Through this study, we will measure the nonlinearity of ENSO obtained from each CGCM and investigate the relationship between NDH and skewness of ENSO, to see whether our finding from the observation is also consistently shown in the coupled GCM model. The analysis of the nonlinearity of model ENSO provides another test for improving the model.

2. Nonlinearity of ENSO from CMIP

One measure for the ENSO nonlinearity is the skewness. The skewness by definition is a measure of the asymmetry of a probability distribution function and is zero for a normal distribution (White 1980). Several observational studies pointed out that the ENSO index (i.e., Niño-1, -2, -3, -3.4) is distinguishable from a Gaussian distribution and the eastern Pacific SST anomalies are positively skewed (Trenberth 1997; Burgers and Stephenson 1999; Hannachi et al. 2003), and the positive skewness is attributed to the nonlinearity (Jin et al. 2003; An and Jin 2004). The moment coefficient of skewness is defined as the normalized third statistical moment (skewness = $m_3/(m_2)^{3/2}$). Thus, the small standard deviation can cause the large skewness. To avoid this, we examine "asymmetricity" rather than skewness, which is the variance-weighted skewness. Asymmetricity is defined as follows:

$$\text{asymmetricity} = \frac{m_3}{(m_2)^{1/2}}, \tag{1}$$

where m_k is the kth moment,

$$m_k = \sum_{i=1}^{N} \frac{(x_i - \overline{X})^k}{N},$$

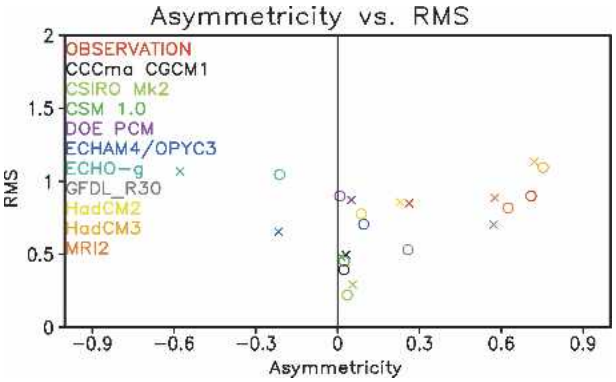

FIG. 1. Scatterplot of the rms vs asymmetricity of the Niño-3.4 (×) and Niño-3 (○) indices generated by results from CMIP simulations and observations. The value for the observed ENSO indices is obtained for the period 1950–2001. Units for the rms and asymmetricity are °C and °C^2, respectively.

and where x_i is the ith observation, $\overline{X}$ is the mean, and N is the number of observations. The statistical significance can be estimated from the standard error (SE) of asymmetricity (SE = $m_2\sqrt{24/L}$ is associated with the 95% confidence level) depending on the number of independent samples (L) in an analyzed variable (White 1980). Here, the numbers of independent samples are determined by the Monte Carlo technique (Livezey and Chen 1983).

Figure 1 shows the root-mean-square (rms) and asymmetricity of SST anomalies over Niño-3 (5°S–5°N, 150°–90°W) and Niño-3.4 (5°S–5°N, 170°–120°W) regions obtained from CMIP and observations. The observed SST data are obtained from the National Centers for Environmental Prediction (NCEP), and its sample consists of monthly means from January 1950 to December 2002. The general information regarding each model output is summarized in Table 1. Anomalies are calculated by removing the climatological mean. The model asymmetricity differs widely from one model to another. The first version of the Canadian Centre for Climate Modelling and Analysis Coupled Global Climate Model (CCCma-CGCM1), Climate System Model (CSM1.0), the Commonwealth Scientific and Industrial Research Organisation (CSIRO) model [CSIRO-Mark 2 (Mk2)], ECHAM4/OPYC3, the Second Hadley Centre Coupled Ocean–Atmosphere General Circulation Model (HadCM2), and the Department of Energy Parallel Climate Model (DOE-PCM) have small asymmetricity and are similar to the normal distribution, inferring that they are underestimating the nonlinearity of ENSO. ECHAM/Hamburg Ocean Primitive Equation model (HOPE-g) (ECHO-g) and ECHAM4/OPYC3 produced the negatively skewed ENSO, indicating that the cold events are unrealistically stronger than the warm events, especially in the Niño-3.4 region. Only the Geophysical Fluid Dynamics Laboratory's model (GFDL_R30), the second Meteorological Research Institute model (MRI2), and HadCM3 have a positive asymmetricity as large as that observed. There is a slight positive correlation tendency between rms and asymmetricity.

Figure 2 shows the spatial distribution of the asymmetricity of SST anomalies obtained from each coupled model output. Again, the asymmetricity distribution of each model widely differs from one another. In the observation, a large positive asymmetricity with the maximum at the near east coast is observed in the eastern Pacific. The asymmetricity distribution appears to be directly related to the ENSO pattern, suggesting that the warm SST anomaly in the equatorial Pacific is stronger than the cold SST anomaly. The MRI2 model especially produced the asymmetricity pattern most similar to the observation among 10 CGCMs. The asymmetricity of the ENSO index obtained from GFDL has a similar value to that observed, but the positive asymmetricity is mainly confined between the date line and 120°W. In both CSIRO-Mk2 and CCCma-CGCM1, the asymmetricity is close to zero over the whole tropical Pacific. The CSM1.0 and the DOE-PCM show very weak positive asymmetricity over the western equatorial Pacific, and the HadCM2 show the negative asymmetricity in the tropical western Pacific and the positive asymmetricity in the tropical central Pacific. The strong negative asymmetricity over the equatorial Pacific is observed from the ECHO-g. The ECHAM4/OPYC3 shows a dipole structure of asymmetricity over the eastern Pacific.

Every CGCM shown in Fig. 2 underestimates the asymmetricity near the eastern boundary, and some models capture the large asymmetricity over the central Pacific. The weak asymmetricity near the eastern boundary may be related to the warm climatological-mean SST bias in that region—possibly due to the weak coastal upwelling—which commonly appeared in most CGCMs (Mechoso et al. 1995; Latif et al. 2001). The maximum positive SST anomaly that can occur during El Niño, can be theoretically identified as the difference between the climatological-mean SST and the theoretical upper limit of SST (the radiative–convective equilibrium temperature of about 30°C), the so-called maximum potential intensity (MPI; Jin et al. 2003; An and Jin 2004). Because of the warm bias, the maximum positive SST anomaly in CGCM near the eastern boundary is much smaller than the observed, and thus the difference in the amplitude between El Niño and La Niña may not be much larger than observed. Therefore,

TABLE 1. Model descriptions. Heat, freshwater, and momentum flux adjustment corrections are H, W, and M, respectively.

	Atmosphere–ocean models	Data length (yr)	Std of Niño-3.4	Asymmetricity of Niño-3.4	Resolutions of atmosphere–ocean models	Flux adjustment	Vertical coordinate
CCCma-CGCM1	GCM2/GFDL MOM1.1	80	0.498	0.0310	T32, L10/1.8 × 1.8, L29	H, W	*Z*
CSIRO-Mk2	CSIRO nine-level AGCM/Bryan–Cox primitive equation	100	0.292	0.0559	R21, L9/3.2 × 5.6, L21	H, W, M	*Z*
CSM1.0	CCM3.0/NCOM1.0	300	0.483	0.01265	T42, L18/2.0 × 2.4, L45		*Z*
DOE-PCM	CCM3/LANL POP	300	0.873	0.0508	T42, L18/0.67 × 0.67, L32		*Z*
ECHAM4/OPYC3	ECHAM/OPYC GCM	240	0.654	−0.2166	T42, L19/2.8 × 2.8, L11	H, W	Isopycnal
ECHO-g	ECHAM/HOPE-g	100	1.069	−0.5767	T30, L19/T42, L20	H, W	Isopycnal
GFDL_R30	GFDL/GFDL MOM 1.1	300	0.702	0.5728	R30, L14/1.875 × 2.25, L18	H, W	*Z*
HadCM2	Unified model/Bryan–Cox primitive equation	80	0.858	0.2296	2.5 × 3.75, L19/2.5 × 3.75, L20	H, W	*Z*
HadCM3	Unified model/Bryan–Cox primitive equation	80	1.132	0.7205	2.5 × 3.75, L19/1.25 × 1.25, L20		*Z*
MRI2	MRI JMA98/Bryan–Cox primitive equation	80	0.887	0.5768	T42, L30/2.0 × 2.5, L28	H, W, M	*Z*

the CGCM, which has the warm bias in near the eastern boundary, mostly produces the weak asymmetricity of SST.

The amplitude of ENSO would be normally distributed if the coupled ocean–atmosphere were a linear system forced by the weather noise (e.g., Thompson and Battisti 2000). (There are two types of the stochastic forcing: one is additive and the other is multiplicative. Here, we specifically refer to the linear model with the additive stochastic forcing. When the multiplicative stochastic forcing is incorporated to the model, the model is no longer linear.) On the other hand, the amplitude of ENSO would be skewed either positively or negatively if the coupled ocean–atmosphere were a nonlinear system. (If a coupled model is nonlinearly formulated but its linear stability is in a stable regime, then the model cannot produce the asymmetry, because the nonlinearity cannot be operating under the subcritical regime. Thus, "a nonlinear system" here particularly indicates that the system is linearly unstable.) The ENSO during the pre-1980s seems to belong to the linear system, while that during the post-1980s belong to the nonlinear system, since the observed nonlinearities such as the skewness of SST and NDH have significantly increased during the post-1980s (Jin et al. 2003; An and Jin 2004; An et al. 2005). In this sense, the CGCM simulating the skewed ENSO is expected to produce a large NDH. Here, we investigate the relationship between the NDH and the asymmetricity. The NDH is defined in the following SST equation for the heat budget of the ocean surface layer:

$$\frac{\partial T'}{\partial t} = -(u'\partial x\overline{T} + v'\partial y\overline{T} + w'\partial z\overline{T} + \overline{u}\partial xT' + \overline{v}\partial yT' + \overline{w}\partial zT') - (u'\partial xT' + v'\partial yT' + w'\partial zT') + R', \quad (2)$$

where T, u, v, and w, are SST, zonal, meridional, and vertical velocities, respectively. The overbars and primes denote the climatological means and anomalies, respectively. Surface heat flux and subgrid-scale contributions (e.g., small oceanic diffusion, heat flux due to tropical instability wave, etc.) are attributed to the residual term R. The second bracketed term of Eq. (2) indicates NDH. To evaluate the role of NDH, we calculated the heat budget in the uppermost 50-m layer of the tropical Pacific.

Here, we calculate the mean NDH and asymmetricity of SST anomaly over the Niño-3 and Niño-3.4 regions. The zonal and meridional currents, and temperature in the ocean subsurface for the calculation of NDH are only available for CSIRO Mk2, GFDL_R30, HadCM3, and MRI2; thus the five-model outputs and observation are utilized for this calculation. Figure 3 shows a relationship between NDH and asymmetricity. In general, the large asymmetricity corresponds to the large NDH, except in HadCM3. The large asymmetricity of HadCM3 may be attributed to other nonlinear processes such as other nonlinear atmospheric responses (see discussion in An and Jin 2004). Figure 3 confirms that the asymmetry of ENSO is mainly due to the NDH. Note that the range of one standard devia-

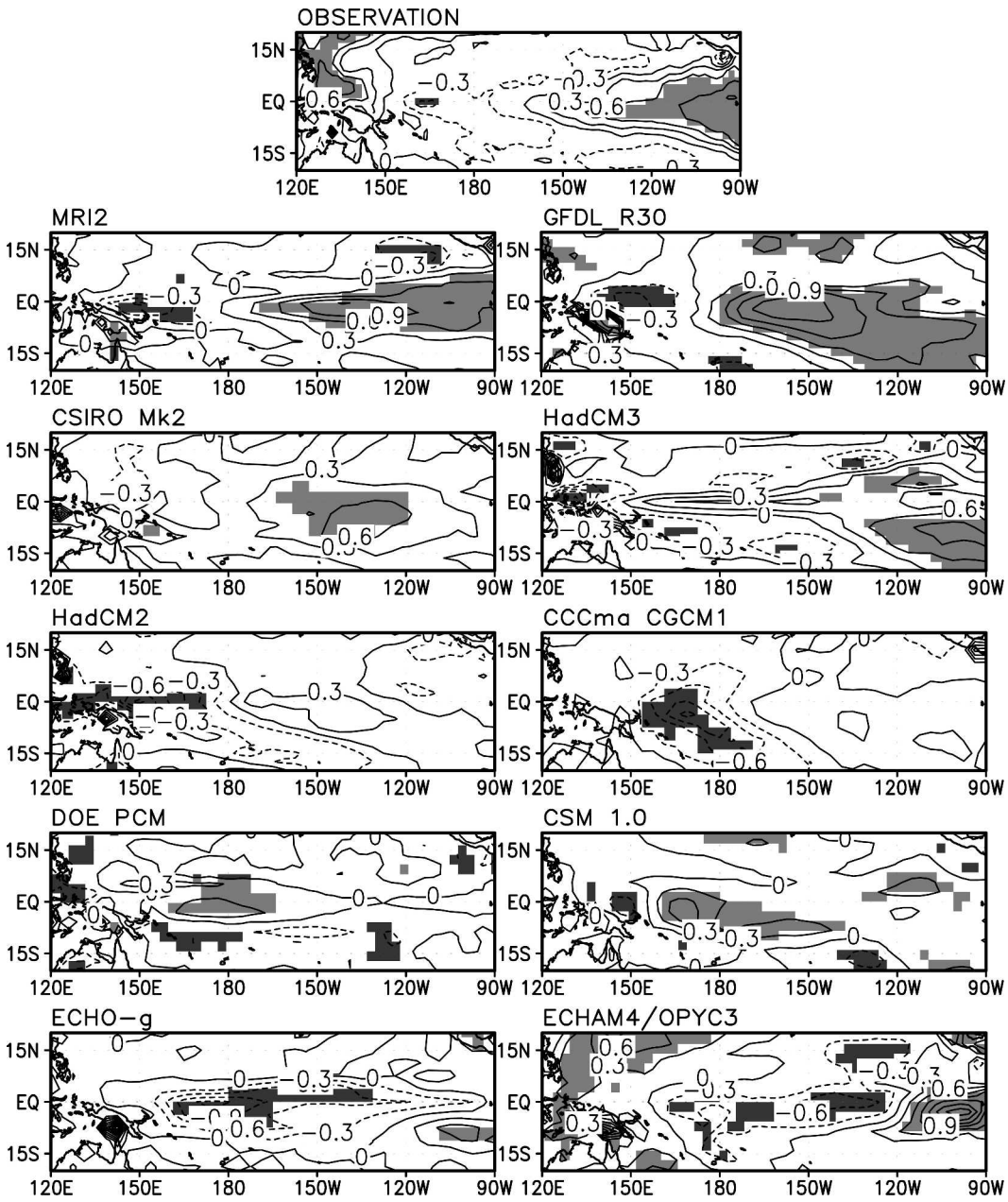

FIG. 2. Spatial distribution of asymmetricity for the monthly mean SST anomalies in the tropical Pacific. Each model code and the observations (OBS) are indicated at the upper-right corner. The areas over the 95% confidence level are shaded. Units are $°C^2$.

tion of NDH shown in Fig. 3 implies that NDH is generally a positive value.

3. Propagation, intensity, and NDH

In the previous section, we found that among 10 CGCMs, the MRI2 coupled GCM best simulates the asymmetricity (and skewness) pattern of the observation. Here, we analyze the MRI2 outputs in detail to see whether the MRI2 outputs are consistent with the observation, especially regarding the NDH, intensity, and propagation.

Figure 4 shows the time series of the SST anomaly and the NDH over 2°S–2°N and 170°–120°W obtained from the MRI2 simulation. It has many features similar to the observation. For example, the El Niño is stronger

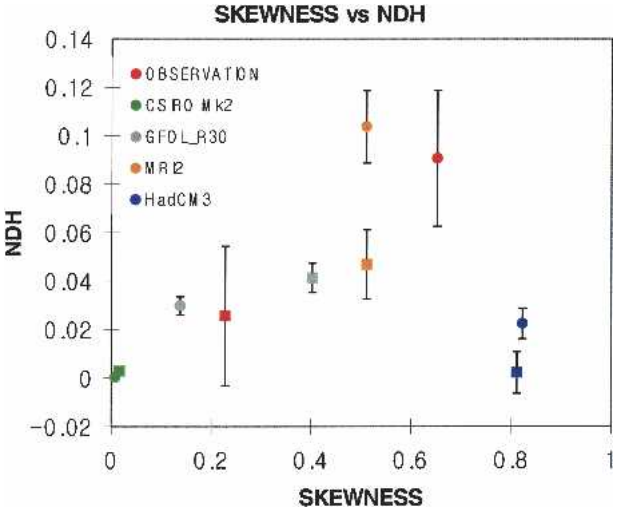

FIG. 3. Scatterplot of asymmetricity vs NDH averaged over the Niño-3 (●) and Niño-3.4 (■) regions generated by results from CMIP simulations and observations. Units for asymmetricity and NDH are °C^2 and °C month^{-1}, respectively. The error bar indicates one standard deviation of the 24-month running NDH.

than La Niña, inferring the positive skewness; NDH is thoroughly positive, and the strong El Niño is accompanied by the strong NDH, while the NDH for the weak El Niño is small. It is also observed in Fig. 4 that the strong positive NDH appears not only during the warm phase but also during the cold phase, implying that the NDH amplifies the warming for the El Niño and dwarfs the cooling for the La Niña; thus, the El Niño is stronger than La Niña.

Jin et al. (2003) and An and Jin (2004) showed that the amplitude of NDH is related to the direction of the movement of the ENSO: when it moves eastward, NDH becomes large; when it moves westward, NDH is

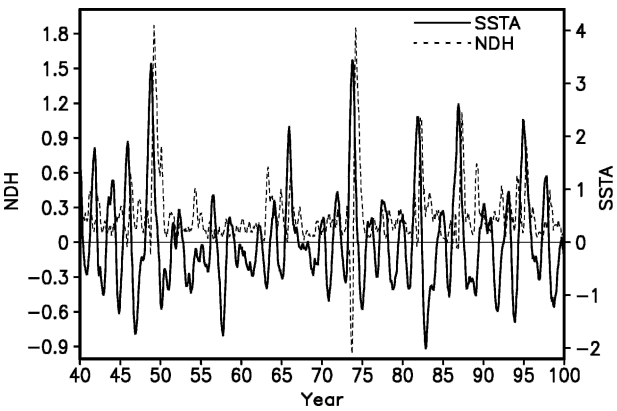

FIG. 4. Time series of SST anomaly (°C) (solid line) and SST tendencies (°C month^{-1}) (dashed line) due to the nonlinear dynamical heating averaged over 2°S–2°N, 170°–120°W. The 5-month running mean has been applied.

small. This is because the anomalous current/upwelling and temperature gradient can be strongly correlated when the system associated with ENSO moves eastward. To see whether MRI2 shows a similar feature, we first draw the composite maps of SST anomalies, subsurface temperature anomalies, and NDH of six strong and nine weak El Niño events. The strong (weak) El Niño events are defined as the cases in which the Niño-3.4 SST is greater than 2.5°C (0.5°–1°C) during the boreal winter.

As shown in Fig. 5, both equatorial SST and subsurface anomalies associated with the strong El Niño tend to propagate to the east, while those associated with the weak El Niño tend to move to the west. In addition, for the strong, eastward-moving El Niño, the subsurface temperature anomalies lead the SST anomalies by about 4–6 months, and thus the large phase difference (about a quarter cycle) between the surface temperature anomaly and subsurface temperature anomaly are maintained during the ENSO evolution. It causes the large vertical temperature gradient. As a result, NDH could be larger (especially due to $-w'T'_z$). On the other hand, for the weak, westward-moving El Niño, the subsurface temperature anomalies are almost in phase with the SST anomalies, causing a small vertical temperature gradient, consequently a small NDH. The relationship between the propagating direction of the ENSO and the NDH is verified in both models and observations (see Figs. 8 and 9 of An and Jin 2004). Note that the negative NDH during the developing phase of ENSO is due to the zonal advection of SST anomaly by the anomalous zonal current ($-u'T'_x$). During the developing phase of El Niño, the anomalous zonal temperature gradient in the ocean surface layer is positive and the anomalous zonal current in the surface layer is positive; thus, the SST tendency due to the nonlinear zonal advection becomes negative. However, the nonlinear zonal advection obtained from the NCEP and Simple Ocean Data Assimilation (SODA) datasets was commonly positive because the anomalous zonal current in the surface layer is negative. In MRI2, the Ekman current that is directly driven by the surface wind may be stronger than the geostrophic current, and in the ocean assimilation data the opposite is true. Nevertheless, the total NDH in MRI2 is mainly determined by the nonlinear vertical advection ($-w'T'_z$), and the net effect of NDH appearing in the MRI2 is similar to the observation.

4. Decadal changes in ENSO variability

Concurrent with the well-known late 1970s global climate shift, the observed ENSO nonlinearity, especially

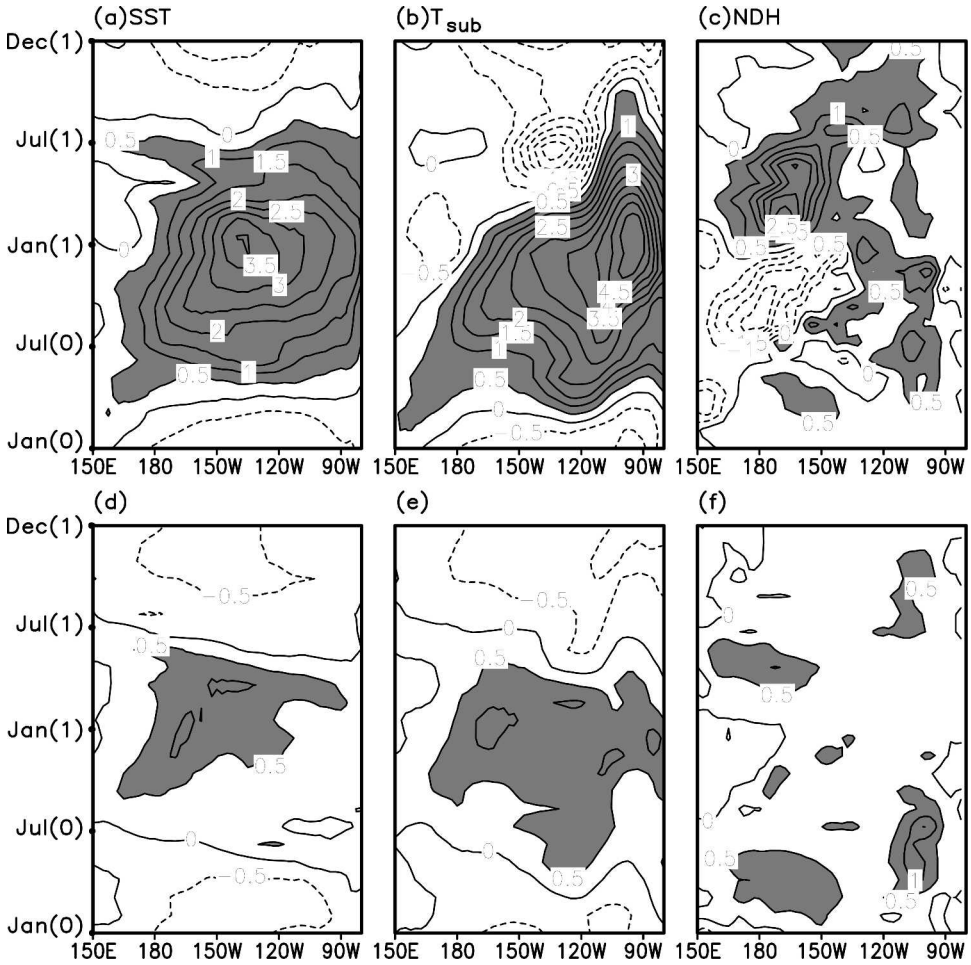

FIG. 5. Composite map in time–longitude section of (a) SST anomalies (°C), (b) subsurface temperature anomalies (°C), and (c) the nonlinear dynamic heating rate (°C month^{-1}) along the equator (1°N–1°S) for six extreme El Niños. (d), (e), (f) The counterparts of nine weak El Niños.

El Niño–La Niña asymmetry, has changed (Wu and Hsieh 2003; An and Jin 2004; An 2004; An et al. 2005). As a possible origin for this change, the nonstationary nature of the climate state (An and Jin 2000; An and Wang 2000; Fedorov and Philander 2000; An and Jin 2004) and the intrinsic nonlinear process of ENSO (Timmermann 2002; Timmermann et al. 2003) have been proposed. Furthermore, several studies suggested that the climate state could even be altered by the ENSO nonlinear process (Jin et al. 2003; Timmermann 2003; An and Jin 2004; Rodgers et al. 2004; An 2004). Nevertheless, the relationship between the climate state and the nonlinearity is not fully investigated (some evidence can be found in Jin et al. 2003). Here, we examine the decadal changes in the skewness of SST anomalies in the tropical Pacific and their relations to the climate state change that appeared in MRI2 and GFDL_R30. The reason to choose these two model results is that they both well simulate the nonlinearity of ENSO as discussed in the previous sections.

To examine the decadal change in the variability of ENSO, the running skewness and variance of SST anomalies, and NDH with the 10-yr window length are calculated. The time series of the running skewness and variance of SST anomalies and NDH from each model are obtained by averaging over the region where the utilized variable is the maximum shown in Fig. 2 [e.g., for the skewness and NDH GFDL (2°S–2°N, 170°E–100°W) and MRI2 (2°S–2°N, 150°–90°W), and for the variance GFDL (3°S–3°N, 160°E–140°W) and MRI2 (3°S–3°N, 180°–100°W)]. Figure 6 shows the time series of the area-averaged 10-yr running skewness and variance of SST anomalies and NDH. The strong decadal changes in the three variables are observed in both MRI2 and GFDL_R30. The decadal changes in skewness are characterized by the large amplitude of about

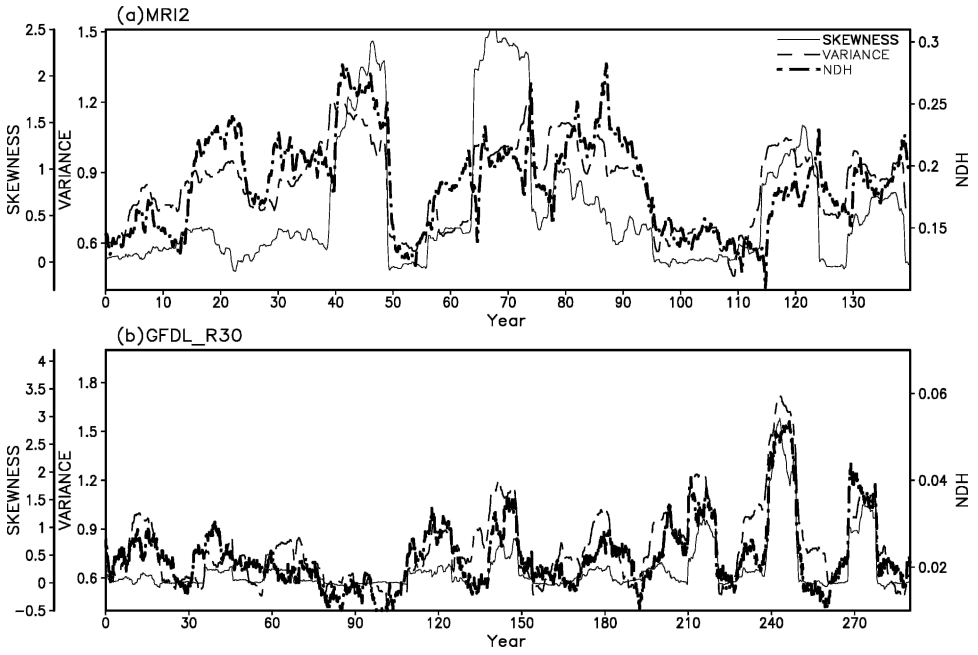

FIG. 6. (a) Time series of the 10-yr running skewness (solid) and variance (dashed) of SST anomalies, and NDH (dot–dashed) over the equatorial Pacific obtained from MRI2 CGCM. (b) Same as in (a) except for GFDL_R30. The area taken for average is indicated in text.

2.3 in MRI2 and about 4.5 in GFDL_R30. Comparison of the running skewness with the running variance yields the high correlation of 0.72 in MRI2 and 0.83 in GFDL_R30. As expected, the running NDH is also highly correlated to both the running skewness and variance. The correlation between the running skewness and NDH is 0.53 in MRI2 and 0.84 in GFDL_R30. These high correlations imply that the decadal period when the positively skewed ENSO events are dominant is associated with the positive NDH and the large amplitude of ENSO. This high correlation would be expected because the nonlinear instability generating a large skewness of ENSO is possible only when the amplitude of ENSO reaches a certain level. In other words, the nonlinear process starts working when the system is linearly unstable so that the amplitude becomes larger than that when it is in the stable regime.

Figure 7 displays the correlation patterns of the 10-yr running SST anomalies and subsurface temperature anomalies at the equatorial section against the area-averaged time series of the 10-yr running skewness (Fig. 6). In both models, the 10-yr running mean of tropical eastern Pacific SST is correlated to the 10-yr running skewness of SST. This east–west contrast correlation pattern is not only pronounced in the surface (SST) but also in the subsurface (e.g., thermocline; Figs. 7c,d). Similar findings but in the different models (ECHAM3/OPYC3 and ECHO-g) were also mentioned by Timmermann (2003) and Rodgers et al. (2004), respectively. They especially showed that the decadal variation of the leading EOF mode of the thermocline depth anomaly, which is characterized by the east–west contrast pattern, is highly correlated to the decadal change in the ENSO amplitude or the decadal change in the El Niño–La Niña asymmetry. Since each CGCM has its own characteristic, the EOF patterns of the thermocline obtained from each model are not identical. However, in general, the deepening of thermocline and the warming of SST in the eastern Pacific are associated with the larger skewness and variance (amplitude) of the eastern Pacific SST anomaly. This is also true as shown in our analysis. Associated with the running positive skewness and large variance, the equatorial eastern Pacific Ocean temperature between the surface and 150-m depth increases, while the equatorial western Pacific Ocean temperature decreases (Figs. 7c,d), which is consistent with the findings from the other models. The possible mechanism to generate this high correlation shown in Fig. 7 is discussed in the following section.

5. Summary and discussion

In this study, we analyzed 10 CGCM results participating in CMIP to investigate the nonlinearity of ENSO. Large differences in the asymmetricity (the

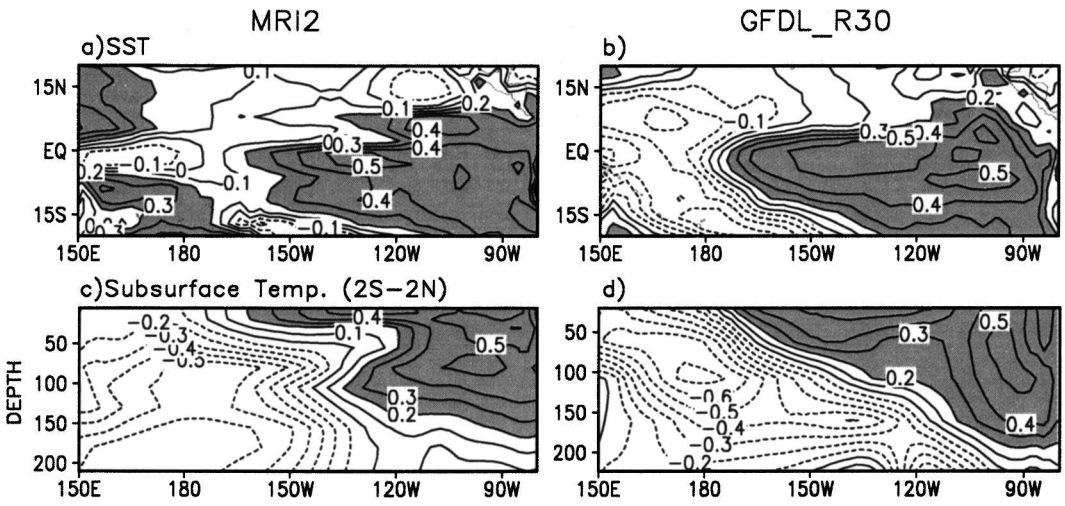

FIG. 7. Correlation map of (a) the 10-yr running mean SST anomaly and (c) ocean temperature at the equatorial section (2°S–2°N) against the time series of the area-averaged 10-yr running skewness shown in Fig. 6. (a), (c) Obtained from MRI2. (b), (d) Same as in (a), (c), respectively, except for GFDL_R30.

variance-weighted skewness) were found between models and observation. CCCma-CGCM2, CSIRO-Mk2, CSM1.0, DOE-PCM, and HadCM2 produced low asymmetricity, indicating the underestimation of the nonlinearity, while ECHAM4/OPY3 (only east of 120°W), MRI2, GFDL_R30, and HadCM3 produced a significant positive asymmetricity. A linear relationship between the asymmetricity and NDH from the independent model outputs was observed, suggesting that the NDH causes the asymmetry of ENSO in most cases. In particular, MRI2, of which ENSO nonlinearity is most similar to that observed, verified that the strong (weak) ENSO events are accompanied by the strong (weak) NDH and they tend to propagate (westward) eastward as seen in the observation.

The differences of the CGCMs in the ENSO nonlinearity are somehow related to the differences in their ocean component. For example, ECHO-g and ECHAM4/OPY3, which show negatively skewed SST in the central Pacific, both use isopycnal levels as a vertical coordinate while the other models use the Z coordinate. In addition, MRI2, GFDL, and HadCM3, which produced more or less reasonable positively skewed ENSO, were developed from the similar ocean model based on Bryan and Cox (1972). Thus, it may imply that the ocean dynamical process is an important factor in determining the nonlinearity of ENSO. Further experiments for this idea need to be pursued.

The significant decadal changes in the skewness and variance of the model-simulated ENSO and NDH were observed as described in section 4, and it is also found that these changes are highly correlated to the decadal variation in the tropical SST. As mentioned by Timmermann (2003), this strong association may have three reasons: 1) a decadal mode causes decadal variations in ENSO variability (i.e., skewness and variance); 2) both decadal ENSO variability and the decadal changes of the background state are generated by one process; and 3) the decadal change in the El Niño–La Niña asymmetry manifests itself as a rectified change in the background state. Among these three reasons, the least possible is 1), because Fig. 7, as well as Timmermann (2003) and Rodgers et al. (2004) showed that the large positive running skewness and variance of SST are associated with the warming in the eastern Pacific and cooling in the western Pacific. This east–west heat contrast pattern is associated with the reduction of the zonal temperature gradient, and the weakening of trade wind, and it also indicates the decrease of vertical temperature gradients in the eastern Pacific. These changes are directly linked to the reduction of the linear instability, obviously resulting in the decrease of the amplitude of ENSO. Thus, if 1) were true, the correlation between the running skewness and variance of SST and the decadal change in the background state of SST would be negative. Thus, although the decadal changes in the high-latitude climate may influence the tropical climate via the oceanic or atmospheric loops (Gu and Philander 1997; Kleeman et al. 1999; Barnett et al. 1999; Pierce et al. 2000; Liu and Yang 2003), it is unclear whether this external decadal influence can synchronize with the decadal change in ENSO variability in the manner that is shown here. On the other hand, 2) and 3) are the strongest possibilities. Regarding 2), Timmermann (2003) showed that the coupled nonlinear dynamics (the so-called homoclinic ENSO dynamics)

could describe both the decadal changes of ENSO variance and the existence of a decadal tropical mode as one dynamical structure, in which the decadal changes in the background state are induced by the nonlinear rectification. In this sense, 2) partly includes 3). Regarding 3), the NDH causes the asymmetry of ENSO, and the long-term accumulated NDH is directly incorporated into the background climate state (Jin et al. 2003). Furthermore, in the observation, the decadal change in the skewness of SSTA in the tropical eastern Pacific was found to be positively correlated to decadal SST variations in the tropical eastern Pacific, again suggesting a nonlinear positive feedback between ENSO variability and mean climate change (An 2004). However, it is unclear what determines the time scale of this mean-variability feedback and what physical process plays the role of switching the sign of the long-term equatorial Pacific SST skewness. Thus, in order to fully understand the underlying mechanism, further studies need to be pursued.

Acknowledgments. The authors would like to thank Dr. G. A. Meehl who kindly provided the CMIP data, as well as two anonymous reviewers and Dr. A. Timmermann for their constructive comments. The first author, An, has been supported by the Japan Agency for Marine-Earth Science and Technology through its sponsorship of the International Pacific Research Center. Ham, Kug, and Kang are supported by the SRC program of Korea Science and Engineering Foundation, the Brain Korea 21 project, and the Ministry of Environment as "The Eco-techonopia 21 Project." Jin was supported by NSF Grant ATM-0226141 and NOAA Grants GC01-229 and GC01246. The authors thank Diane Henderson for editing the manuscript.

REFERENCES

An, S.-I., 2004: Interdecadal changes in El Niño–La Nina asymmetry. *Geophys. Res. Lett.,* **31,** L23210, doi:10.1029/2004GL021699.

——, and F.-F. Jin, 2000: An eigen analysis of the interdecadal changes in the structure and frequency of ENSO mode. *Geophys. Res. Lett.,* **27,** 1573–1576.

——, and B. Wang, 2000: Interdecadal change of the structure of the ENSO mode and its impact on the ENSO frequency. *J. Climate,* **13,** 2044–2055.

——, and F.-F. Jin, 2004: Nonlinearity and asymmetry of ENSO. *J. Climate,* **17,** 2399–2412.

——, W. W. Hsieh, and F.-F. Jin, 2005: A nonlinear analysis of the ENSO cycle and its interdecadal changes. *J. Climate,* in press.

Barnett, T., D. W. Pierce, M. Latif, D. Dommenget, and R. Saravana, 1999: Interdecadal interaction between the tropics and the midlatitude in the Pacific basin. *Geophys. Res. Lett.,* **26,** 615–618.

Battisti, D. S., and A. C. Hirst, 1989: Interannual variability in the tropical ocean–atmosphere system: Influence of the basic state, ocean geometry and nonlinearity. *J. Atmos. Sci.,* **46,** 1687–1712.

Bjerknes, J., 1969: Atmospheric teleconnections from the equatorial Pacific. *Mon. Wea. Rev.,* **97,** 163–172.

Bryan, K., and M. D. Cox, 1972: An approximate equation of state for numerical models of ocean circulation. *J. Phys. Oceanogr.,* **2,** 510–514.

Burgers, G., and D. B. Stephenson, 1999: The "normality" of El Niño. *Geophys. Res. Lett.,* **26,** 1027–1030.

Cane, M. A., and S. E. Zebiak, 1985: A theory for El Niño and the Southern Oscillation. *Science,* **228,** 1084–1087.

Chang, P., L. Ji, H. Li, and M. Flugel, 1996: Chaotic dynamic versus stochastic processes in ENSO in coupled ocean-atmosphere models. *Physica D,* **9,** 301–320.

Fedorov, A. V., and S. G. H. Philander, 2000: Is El Niño changing? *Science,* **228,** 1997–2002.

Gu, D., and S. G. H. Philander, 1997: Interdecadal climate fluctuations that depend on exchanges between the tropics and extratropics. *Science,* **275,** 805–807.

Hannachi, A., D. B. Stephenson, and K. R. Sperber, 2003: Probability-based methods for quantifying nonlinearity in the ENSO. *Climate Dyn.,* **20,** 241–256.

Hsieh, W. W., 2001: Nonlinear principal component analysis by neural networks. *Tellus,* **53A,** 599–615.

——, 2004: Nonlinear multivariate and time series analysis by neural network methods. *Rev. Geophys.,* **42,** RG1003, doi:10.1029/2002RG000112.

Jin, F.-F., 1996: Tropical ocean-atmosphere interaction, the Pacific cold tongue, and the El Niño-Southern Oscillation. *Science,* **274,** 76–78.

——, 1997: An equatorial ocean recharge paradigm for ENSO. Part I: Conceptual model. *J. Atmos. Sci.,* **54,** 811–829.

——, D. Neelin, and M. Ghil, 1994: El Niño on the devil's staircase: Annual subharmonic steps to chaos. *Science,* **264,** 70–72.

——, S.-I. An, A. Timmermann, and J. Zhao, 2003: Strong El Niño events and nonlinear dynamical heating. *Geophys. Res. Lett.,* **30,** 1120, doi:10.1029/2002GL016356.

Kessler, W. S., and M. J. McPhaden, 1995: Oceanic equatorial waves and the 1991–1993 El Niño. *J. Climate,* **8,** 1757–1774.

Kleeman, R., J. P. McCreary, and B. A. Klinger, 1999: A mechanism for generating ENSO decadal variability. *Geophys. Res. Lett.,* **26,** 1743–1746.

Latif, M., and Coauthors, 2001: ENSIP: The El Niño Simulation Intercomparison Project. *Climate Dyn.,* **18,** 255–276.

Liu, Z., and H. Yang, 2003: Extratropical control of tropical climate, the atmospheric bridge and oceanic tunnel. *Geophys. Res. Lett.,* **30,** 1230, doi:10.1029/2002GL016492.

Livezey, R. E., and W. Y. Chen, 1983: Statistical field significance and its determination by Monte Carlo technique. *Mon. Wea. Rev.,* **111,** 46–59.

McCreary, J. P., 1983: A model of tropical ocean-atmosphere interaction. *Mon. Wea. Rev.,* **111,** 370–387.

Mechoso, C. R., and Coauthors, 1995: The seasonal cycle over the tropical Pacific in coupled ocean–atmosphere general circulation models. *Mon. Wea. Rev.,* **123,** 2825–2838.

Moore, A. M., and R. Kleeman, 1999: Stochastic forcing of ENSO by the intraseasonal oscillation. *J. Climate,* **12,** 1199–1220.

Penland, C., and P. D. Sardeshmukh, 1995: The optimal growth of tropical sea surface temperature anomalies. *J. Climate,* **8,** 1999–2004.

Picaut, J., F. Masia, and Y. du Penhoat, 1997: An advective–

reflective conceptual model for the oscillatory nature of the ENSO. *Science,* **277,** 663–666.

Pierce, D. W., T. P. Barnett, and M. Latif, 2000: Connections between the Pacific Ocean Tropics and midlatitudes on decadal time scales. *J. Climate,* **13,** 1173–1194.

Rodgers, K. B., P. Friederichs, and M. Latif, 2004: Tropical Pacific decadal variability and its relation to decadal modulations of ENSO. *J. Climate,* **17,** 3761–3774.

Schopf, P. S., and M. J. Suarez, 1988: Vacillations in a coupled ocean-atmosphere model. *J. Atmos. Sci.,* **45,** 549–566.

Thompson, C. J., and D. S. Battisti, 2000: A linear stochastic dynamical model of ENSO. Part I: Model development. *J. Climate,* **13,** 2818–2832.

——, and ——, 2001: A linear stochastic dynamical model of ENSO. Part II: Analysis. *J. Climate,* **14,** 445–466.

Timmermann, A., 2003: Decadal ENSO amplitude modulations: A nonlinear paradigm. *Global Planet. Change,* **37,** 135–156.

——, and F.-F. Jin, 2002: A nonlinear mechanism for decadal El Niño amplitude changes. *Geophys. Res. Lett.,* **29,** 1003, doi:10.1029/2001GL013369.

——, ——, and J. Abshagen, 2003: A nonlinear theory for El Niño bursting. *J. Atmos. Sci.,* **60,** 152–165.

Trenberth, K. E., 1997: The definition of El Niño. *Bull. Amer. Meteor. Soc.,* **78,** 2771–2777.

Tziperman, E., L. Stone, M. Cane, and H. Jarosh, 1994: El Niño chaos: Overlapping of resonances between the seasonal cycle and the Pacific ocean-atmosphere oscillator. *Science,* **264,** 72–74.

Wang, B., 1995: Interdecadal changes in El Niño onset in the last four decades. *J. Climate,* **8,** 267–285.

——, and S.-I. An, 2001: Why the properties of El Niño changed during the late 1970s. *Geophys. Res. Lett.,* **28,** 3709–3712.

Wang, C., 2001: A unified oscillator model for the El Niño–Southern Oscillation. *J. Climate,* **14,** 98–115.

Weisberg, R. H., and C. Wang, 1997: A western Pacific oscillator paradigm for the El Niño-Southern Oscillation. *Geophys. Res. Lett.,* **24,** 779–782.

White, H. G., 1980: Skewness, kurtosis and extreme values of Northern Hemisphere geopotential heights. *Mon. Wea. Rev.,* **108,** 1446–1455.

Wu, A., and W. W. Hsieh, 2003: Nonlinear interdecadal changes of the El Niño-Southern Oscillation. *Climate Dyn.,* **21,** 719–730.

Wyrtki, K., 1975: El Niño—The dynamic response of the equatorial Pacific Ocean to atmospheric forcing. *J. Phys. Oceanogr.,* **5,** 572–584.

——, 1985: Water displacements in the Pacific and the genesis of El Niño cycles. *J. Geophys. Res.,* **90,** 7129–7132.